Interrogation of a conserved overlap between cofactor and substrate binding domains to facilitate crosstalk-induced conformational changes in Class A Flavin Monooxygenases: A case study of 6-Hydroxynicotinate-3-Monooxygenase

Sam L. Belsky[1], Sipara H. Semu[1], Mark J. Snider[1], Annastassia D. Gallo[1], Zachary R. Turlington[2], Katherine A. Hicks[2]

[1] Department of Biochemistry & Molecular Biology, The College of Wooster, OH; [2] Department of Chemistry, SUNY Cortland, NY

Background & Significance

- Class A FMOs catalyze the stereospecific hydroxylation of aromatic rings, a reaction which is difficult to perform using traditional organic chemistry.
- Utilizing the amazing biosynthetic potential these enzymes possess will allow for the synthesis of new drugs and medications. A recent example of their use can be seen through the first effective synthesis of trichoflectin and lunatoic acid A through the use of FMOs such as TropB, AzaH, AfoD, and SorbC (**Figure 1**).

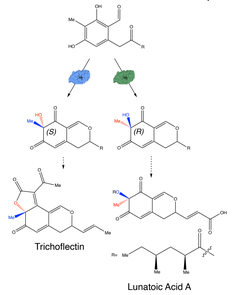

Figure 1 (Left): **Stereo- and regiospecific enzymatic synthesis of scaffolds used in the generation of trichoflectin and lunatoic acid A.** Both chemicals are part of a class of compounds known as azaphilones, which possess a broad range of antimicrobial, antiviral, and anticancer activities. These chemicals can either possess *R*- or *S*-configuration at the C7-position. As shown, the scaffolds required for the synthesis of trichoflecten and lunatoic acid A have distinct stereochemistry at C7, synthesis of these scaffolds was achieved using Class A FMOs.[1]

- During catalysis within this class, the enzyme-bound FAD cofactor undergoes conformational changes taking on *IN* and *OUT* conformations (**Figure 2**). Mobility of the FAD cofactor is critical to catalysis in this class of enzymes so understanding what mechanisms mediate FAD conformational dynamics may help in furthering synthetic applications of these enzymes.

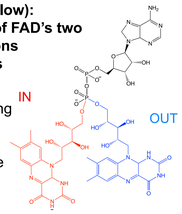

Figure 2 (Right & Below): Structural diagram of FAD's two primary conformations throughout catalysis

- Using structural analysis, we identified a peptide segment (GAG motif) in a subset of these enzymes which likely plays a role in FAD conformational dynamics (**Fig. 3**).

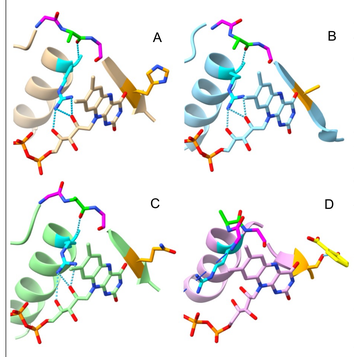

Figure 3: Models of the conserved GAG sequence from the crystal structures of the enzymes (A) NicC, (B) TropB, (C), 3HB6H and (D) SalH. For each structure the GAG sequence is shown with the glycines in pink and the alanines in green. Also shown is a conserved arginine in all four proteins which interacts with the ribityl chain of the FAD. Additional residues reported to undergo direct interactions with bound substrates (orange) are also shown. In the case of structure D, this interaction with the substrate (yellow), likely induces the altered conformational changes in the GAG sequence and conserved arginine.[2,3,4,5]

Research Objectives & Hypotheses

Using the enzyme, 6-hydroxynicotinate-3-monooxygenase (NicC) as a case study, herein I explore the significance of this GAG motif.

- **Hypothesis 1**: Complementary alterations to both substrate and enzyme can be used to alter the specificity of NicC. This is investigated by testing how mutations to H47 alter NicC's interactions with the substrate analogue, 6-amino-nicotinate (6-ANA) (**Figure 4).**
- **Hypothesis 2**: The plasticity of the GAG sequence facilitates conformational changes in response to the binding of the substrate which are critical to FAD conformational dynamics. This is investigated by studying the kinetic implications of altering the plasticity of GAG sequence via site-directed mutagenesis.

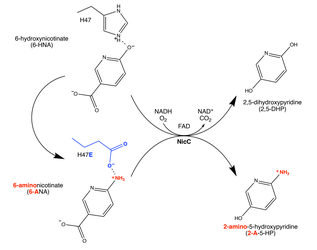

Figure 4: Wild-type NicC and an H47E NicC variant may display distinct substrate specificity. Wild-type NicC catalyzes the decarboxylative hydroxylation of 6-HNA, producing 2,5-DHP using NADH, O_2 and its FAD cofactor. Making complimentary alterations to both the substrate, namely replacing H47 with a glutamate and the hydroxyl moiety of 6-HNA with an amine may facilitate the the decarboxylative hydroxylation of the substrate analogue, 6-ANA.

Variant Stability, Substrate Turnover & Substrate Specificity

Table 1. Stability and ability to turnover substrates of NicC variants

Variant	Stability	Converts 6-HNA into 2,5-DHP	Converts 6-ANA into 2-A-5-HP
WT	Stable	Yes	Yes
G43P	Stable	Yes	N/A
A44G	ND	N/A	N/A
G45A	Unstable	Yes	N/A
H47E	Unstable	No	No
H47Q	Stable	Yes	Yes

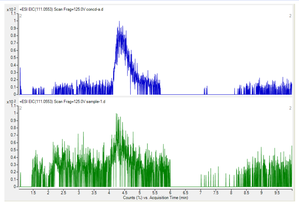

Figure 5 (Above): LC-QTOF-MS Analysis confirmed the formation of 2-amino-5-hydroxypyridine. Data indicated that both the wild-type (green) and H47Q (blue) variant were able to generate this product.

G43P, H47Q & WT NicC Coupling

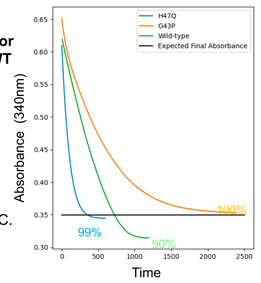

Figure 6 (Right):Time course reaction data for the G43P, H47Q and WT NicC compared to the expected final absorbance. This analysis revealed that both the reaction products generated in G43P and H47Q NicC variants are more coupled than in WT NicC.

Steady State Kinetic Analysis of the G43P & H47Q NicC Variants

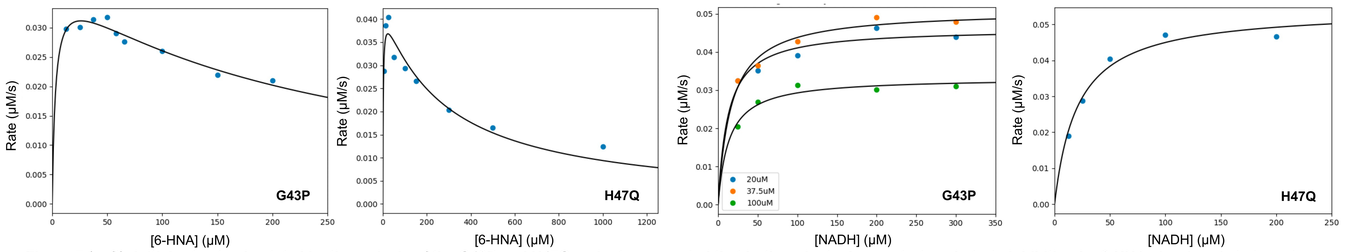

Figure 7 (Left): Initial-rate steady-state kinetic analysis of the G43P and H47Q variants suggested that both variants demonstrate substrate inhibition by 6-HNA. In a bi-substrate system substrate inhibition is fit using **Equation 1** and **Equation 2,** where **Equation 1** is used when the inhibitor concentration is varied and **Equation 2** is used when the concentration of the non-inhibiting substrate is varied. Due to the number of variables in these equations the steady state kinetic parameters could not be accurately determined.

Equation 2

$$v = \frac{V_{max}\cdot[6-HNA][NADH]}{K_{ia}K_M^{NADH} + K_M^{6-HNA}[NADH] + K_M^{NADH}[6-HNA]\left(1+\frac{[6-HNA]K_i}{K_i}\right) + [6-HNA][NADH]}$$

Equation 1

$$v = \frac{V_{max}[6-HNA]}{K_M^{6-HNA}\left(1+\frac{K_{ia}K_M^{NADH}}{K_M^{6-HNA}[NADH]}\right)+[6-HNA]\left(1+\frac{K_M^{NADH}}{[NADH]}\left(1+\frac{[6-HNA]}{K_i}\right)\right)}$$

Kinetics of Substrate Binding in the G43P Variant

Figure 8 (Below): ITC Analysis of the G43P NicC variant. This assay was performed in two buffers with different ΔH_{ion} ((A) Phosphate Buffer, (B) Tris/Acetate Buffer). That difference induced a 70-fold increase in the overall value of $\Delta H_{binding}$, indicating that ionization of the substrate occurs upon binding to the enzyme.

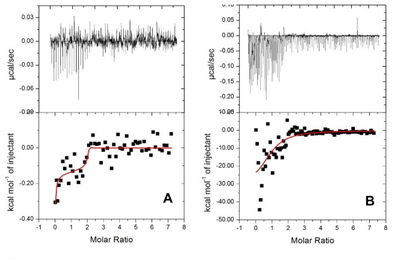

Figure 10 (Right & Below): Stopped-flow kinetic analysis of 6-HNA binding by G43P NicC Stopped flow data tracking perturbations in the 450 nm absorbance signal were fit to a single exponential (A). Analysis of the actual amplitude values ($|A_f - A_0|$) (orange) reveals a slight decrease in amplitude beginning at 2000μM, more indicative of a second binding event.

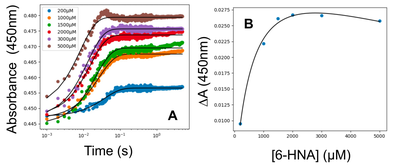

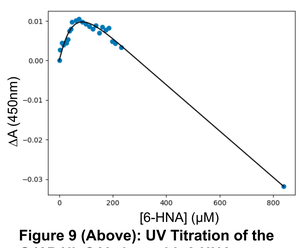

Figure 9 (Above): UV Titration of the G43P NicC Variant with 6-HNA. Changes in the absorbance at 450 nm upon the addition of 6-HNA revealed that this variant binds two molecules of 6-HNA, with the first binding event inducing an increase in absorbance, while the second binding event induced a dramatic decrease in absorbance.

Figure 11 (Below): G43P NicC Variant Catalytic Mechanism. The 2nd 6-HNA binding event likely occurs at the NADH binding domain prior to the binding of the coenzyme.

G43P Stopped-Flow Reduction Kinetics

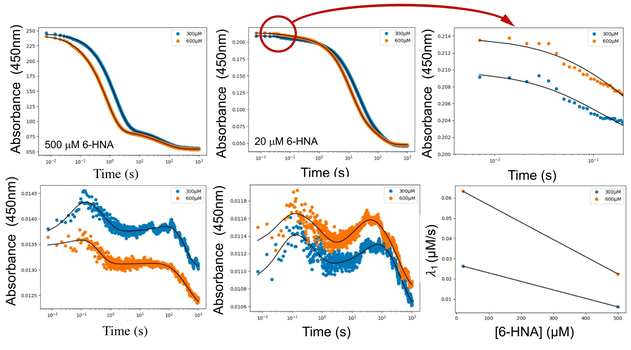

Figure 12 (Above): Kinetics of the Reduction Half-Reaction of G43P by Stopped Flow UV-Vis Spectroscopy Indicate 6-HNA Inhibition is directed toward the binding of NADH. Analysis of 450 nm data suggests that the rate of reduction in the G43P variant is directly related to inhibition. However, more intensive analysis revealed that the signals from the initial reduction event at the lower 6-HNA concentration were so small that analytical fitting disregarded the initial signal. After demonstrating the unreliability of the time course followed at 450 nm, the 590 nm data, used to measure the formation of the charge transfer complex (CTC), demonstrated that the rate of reduction decreases at higher 6-HNA concentrations.

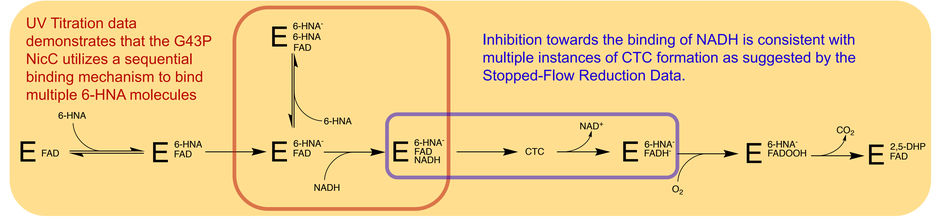

G43P Structural Analysis

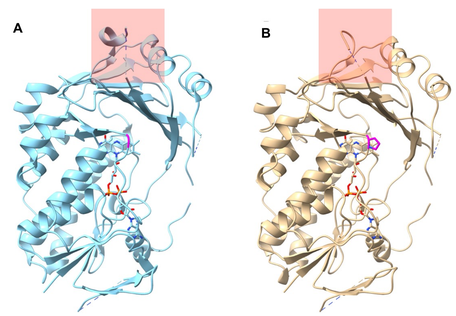

Figure 13: Crystal structures of the G43P and wild-type NicC proteins. The pink highlights the residues at position 43 in both proteins. The red highlights the only significant structural difference between the two structures: an alpha-helix seen in the wild-type protein is shown as a random loop in the G43P structure.

Conclusions

- 6-amino-nicotinate is not a NicC effector, but rather is a poor NicC substrate.
- Due to the manner NicC's use of tunnel in binding substrates altering specificity will require more than simple active site mutations
- Mutations to the GAG motif disturb the mechanism used to trigger conformational changes in the 6-HNA/NADH binding domain. The failure to undergo such conformational changes allows the protein to bind another molecule of 6-HNA at this domain, resulting in substrate inhibition.
- The conservation of this motif, along with its significance towards NicC's binding of NADH suggests that unlike what is implied by most literature on the topic, this subclass of Class A FMOs likely possess a conserved binding domain
- Conformational changes in the NADH binding domain are not required for the formation of the charge-transfer-complex (CTC) intermediate.

Future Work

Kinetics of the G43P and H47Q NicC Variants

- Further elucidate the mechanisms of substrate inhibition in the G43P and H47Q NicC variants and develop a more quantitative basis for the impact that the G43P and H47Q mutations have on the kinetics of NicC.

Conserved Coenzyme Binding Site & Pose

- Since this substrate binding tunnel in NicC is not present in other enzymes with the GAG sequence, the coenzyme binding pose likely involves the nicotinamide ring entering NicC's larger cavity which is universally conserved in this class of enzymes (**Figure 14**), rather than the unconserved 6-HNA binding tunnel from previous hypotheses.

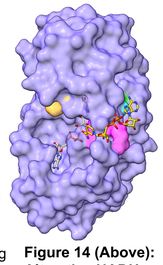

Figure 14 (Above): Alternative NADH binding pose.

Substrate Promiscuity

- Identify the determinants of substrate turnover and coupling in NicC, with an emphasis towards the role of the ionization and inductive effects imposed by the C(6) functional group.

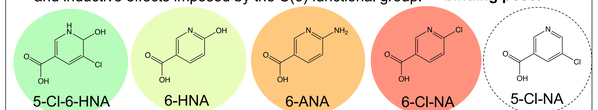

Acknowledgements

- **NSF Grant #1817535**
- LCMS product analysis collaboration with Prof. Jennifer Faust (Wooster)

References

Pyser, J. B.; Baker Dockrey, S. A.; Benitez, A. R.; Joyce, L. A.; Wiscons, R. A.; Smith, J. L.; Narayan, A. R. H. Stereodivergent, Chemoenzymatic Synthesis of Azaphilone Natural Products. *J. Am. Chem. Soc.* **2019**, *141* (46), 18551–18559. https://doi.org/10.1021/jacs.9b09385. (1)

Hicks, K. A.; Yuen, M. E.; Zhen, W. F.; Gerwig, T. J.; Story, R. W.; Kopp, M. C.; Snider, M. J. Structural and Biochemical Characterization of 6-Hydroxynicotinic Acid 3-Monooxygenase, A Novel Decarboxylative Hydroxylase Involved in Aerobic Nicotinate Degradation. *Biochemistry* **2016**, *55* (24), 3432–3446. https://doi.org/10.1021/acs.biochem.6b00206. (2)

Rodríguez Benítez, A.; Tweedy, S. E.; Baker Dockrey, S. A.; Lukowski, A. L.; Wymore, T.; Khare, D.; Brooks, C. L.; Palfey, B. A.; Smith, J. L.; Narayan, A. R. H. Structural Basis for Selectivity in Flavin-Dependent Monooxygenase-Catalyzed Oxidative Dearomatization. *ACS Catal.* **2019**, *9* (4), 3033–3040. https://doi.org/10.1021/acscatal.8b04575. (3)

Montersino, S.; Orru, R.; Barendregt, A.; Westphal, A. H.; van Duijn, E.; Mattevi, A.; van Berkel, W. J. H. Crystal Structure of 3-Hydroxybenzoate 6-Hydroxylase Uncovers Lipid-Assisted Flavoprotein Strategy for Regioselective Aromatic Hydroxylation. *Journal of Biological Chemistry* **2013**, *288* (36), 26235–26245. https://doi.org/10.1074/jbc.M113.479303. (4)

Kita, A.; Watanabe, Y.; Adachi, M.; Kuroki, R.; Morimoto, Y. The Catalytic Mechanism of Decarboxylative Hydroxylation of Salicylate Hydroxylase Revealed by Crystal Structure Analysis at 2.5 Å Resolution. *Biochemical and Biophysical Research Communications* **2016**, *469* (2), 158–163. https://doi.org/10.1016/j.bbrc.2015.11.087. (5)